JACS
JOURNAL OF THE AMERICAN CHEMICAL SOCIETY

Article

pubs.acs.org/JACS

Concentration-Dependent Supramolecular Engineering of Hydrogen-Bonded Nanostructures at Surfaces: Predicting Self-Assembly in 2D

Artur Ciesielski,[†] Paweł J. Szabelski,*[,‡] Wojciech Rżysko,[§] Andrea Cadeddu,[†] Timothy R. Cook,[∥] Peter J. Stang,*[,∥] and Paolo Samorì*[,†]

[†]Nanochemistry Laboratory, ISIS & icFRC, Université de Strasbourg & CNRS, 8 allée Gaspard Monge, 67000 Strasbourg, France

[‡]Department of Theoretical Chemistry and [§]Department for the Modeling of Physico-Chemical Processes, Maria-Curie Skłodowska University, Pl. M. C. Skłodowskiej 3, 20-031 Lublin, Poland

[∥]Department of Chemistry, University of Utah, 315 South 1400 East, Salt Lake City, Utah 84112, United States

Supporting Information

ABSTRACT: We report a joint computational and experimental study on the concentration-dependent self-assembly of a flat C_3-symmetric molecule at surfaces. As a model system we have chosen a rigid molecular module, 1,3,5-tris(pyridine-4-ylethynyl)benzene, which can undergo self-association via hydrogen bonding (H-bonding) to form ordered 2D nanostructures. In particular, the lattice Monte Carlo method, combined with density functional calculations, was employed to explore the spontaneous supramolecular organization of this tripod-shaped molecule under surface confinement. We analyzed the stability of different weak H-bonded patterns and the influence of the concentration of the starting molecule on the 2D supramolecular packing. We found that ordered, densely packed monolayers and 2D porous networks are obtained at high and low concentrations, respectively. A concentration-dependent scanning tunneling microscopy investigation of the molecular self-assembly at a graphite−solution interface revealed supramolecular motifs, which are in perfect agreement with those obtained by simulations. Therefore, our computational approach represents a step forward toward the deterministic prediction of molecular self-assembly at surfaces and interfaces.

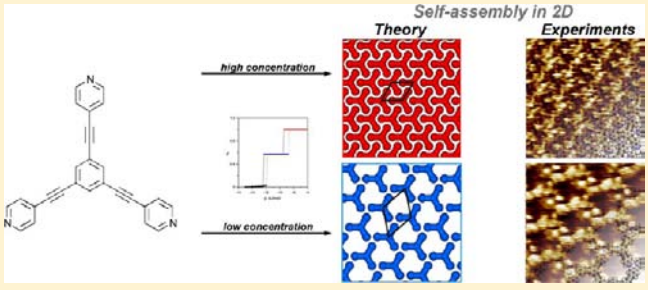

INTRODUCTION

The self-assembly of molecular components into larger supramolecular architectures is ubiquitous in nature and constitutes one of the most powerful methods to fabricate functional nanomaterials by exploiting the bottom-up approach.[1] When spatial confinement in two-dimensions on a solid substrate is employed, this approach can be exploited to generate periodically ordered 2D structures from suitably designed molecular building blocks.[2] Hence, self-assembly at the interface enables the defined positioning of functional entities with subnanometer precision over areas of micrometers and thereby allowing the fine-tuning of numerous properties of the resulting nanostructure[3] for technological applications, in particular in electronics and optics.[4] To allow for structure formation under thermodynamic control, i.e., to warrant equilibration, the use of weak yet multiple noncovalent interactions has proven advantageous. Single noncovalent interactions are typically reversible, owing to their weak bond strength; however, once aggregated across an entire assembly, the sum of these relatively weak interactions manifests in robust materials with self-healing characteristics.[5]

Among the numerous examples of supramolecular arrays on solid surfaces, which have been reported to date,[2a,6] those featuring void spaces, so-called 2D porous networks, are of special importance. The main reason for the growing interest in such periodic architectures, either assembled on metals[7] or graphite,[3e,8] is their great potential for technological applications in nanoengineering and, more generally, in nanotechnology.[2b] A distinct advantage of porous networks is their regular spatial arrangement of nanometer-sized cavities with uniform, well-defined shapes that can be used for storage functions or to control reactivities.[9] Engineering the structure and function of 2D porous networks requires control over structural features of precursors, i.e., shape, nature, and position of interacting sites, as well as molecular electronic properties and the overall topology of the material. This strategy, known as crystal engineering, has rapidly developed for 2D systems.[6e,10] The spontaneous organization of molecular building blocks into planar, periodic supramolecular architectures is driven by inter- and intramolecular forces as well as by interfacial interactions. The resulting 2D networks are typically stabilized by H-bonds,[11] metal−ligand coordination,[12] or van der Waals interactions.[10d,13]

Received: January 8, 2013
Published: April 16, 2013

   dx.doi.org/10.1021/ja4002025 | J. Am. Chem. Soc. 2013, 135, 6942−6950

Hydrogen bonding is one of the most employed noncovalent interactions in supramolecular chemistry.[14] In particular, preprogramming complementary H-bonding sites to guide a system to a specific organization of precursors is the most straightforward pathway for the rational self-assembly of 2D supramolecular porous networks.[15] Moreover, H-bonding can adopt a wide range of energies, depending on the nature, the number (i.e., multiplicity), and the position of consecutive H-bond donor and acceptor moieties, which determine the magnitude of both primary and secondary interactions. While the use of relatively strong, complementary H-bonds leads to the formation of polycrystalline structures, weak H-bonds can readily direct the formation of 2D crystalline structures by taking advantage of their reversible nature.[11i,15c,16] Surprisingly, for some systems the use of single-site H-bonding is sufficiently robust for the engineering of 2D porous networks. Despite its relatively weak interaction energy, the N(pyridyl)···H−C-(pyridyl/aryl) H-bonding motif has been used to drive the formation of 2D supramolecular structures on solid inert surfaces.[17] Noteworthy, these interactions may alternatively be interpreted as weak dipole−dipole or H-bond donor−acceptor motifs as described by Dunitz.[18]

Computer simulations offer an alternative and complementary path to study the self-assembly of functional molecules into 2D ordered supramolecular architectures on solid surfaces.[19] Engineering methods based on all-atom molecular dynamics (MD)[11k,20] and density functional theory (DFT)[21] have recently been devised to predict 2D self-assembly and the formation of supramolecular architectures. These methods were shown to be useful in bridging the gap between the chemical nature of the self-assembly modules (i.e., the supramolecular "genotype") and the structural and dynamic properties (i.e., its "phenotype") of the resulting architecture. Another powerful, yet underestimated, simulation technique in the field of 2D crystal engineering is the Monte Carlo (MC) method, which offers the possibility of investigating large molecular systems under variable conditions. Significantly, this technique makes it possible to mimic self-organization of molecules into naturally emerging 2D patterns without imposing any constraints on the symmetry of the final supramolecular architecture. Furthermore, the MC method is able to predict the coexistence of different phases and to provide information about the conditions under which of these phases are stable. The robustness of the MC method is particularly evident in lattice models in which the substrate and adsorbed molecules are represented in a simplified way.[22] While the concentration-dependent formations of monocomponent supramolecular architectures have been investigated in the past by scanning tunneling microscopy (STM) at the solid−liquid interface,[10d,16d,21c,23] and their results used to gain insight into the thermodynamics of physisorption at surfaces;[13g] MC simulations have hitherto not been utilized to predict concentration-dependent self-assembly.

In this work we employ simple MC simulations, validated with DFT calculations, to effectively model and predict the concentration-dependent self-assembly of achiral molecules adsorbed on a solid surface. Computational evidence has been corroborated experimentally by STM imaging of the self-assembly system at the solid−liquid interface. We focused our attention on 1,3,5-tris(pyridine-4-ylethynyl)benzene (**1**; Scheme 1), which consists of three pyridyl groups connected to a central aryl ring through alkynyl moieties.

Scheme 1. Chemical Structure of 1

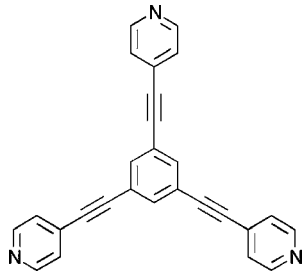

The planar 120° tritopic nature of this molecule has motivated its use in a number of discrete supramolecular coordination complexes.[24] While the terminal pyridyl groups provide Lewis basic sites for coordination chemistry with metal ions, here they are used to orient weak H-bond interactions through N(pyridyl)···H−C(pyridyl/aryl) motifs. Though the coordination of **1** molecules with metallic surfaces has been recently investigated under ultrahigh vacuum conditions,[25] the formation of supramolecular architectures based on weak H-bonding between **1** molecules has been not reported.

EXPERIMENTAL SECTION

The model complex **1** was prepared using literature procedures for the coupling of 1,3,5-triethynylbezene with 4-bromopyridinium chloride.[26]

DFT. All calculations were performed using the using the Becke three-parameter hybrid exchange functional combined with the Lee−Yang−Parr correlation functional (B3LYP)[27] with the 6-311G(d,p)[28] basis sets applied for geometry optimizations. The H-bonding energy was calculated by using formula described in eq 1:

$$\Delta E_{bond} = \Delta E_{total} - \Delta E_{mon} \quad (1)$$

where ΔE_{total} is the total energy of the system computed after minimization of supramolecular structures and ΔE_{mon} is a sum of the energy of monomeric units.

MC SIMULATIONS

Simulations were performed on a $L \times L$ rhombic fragment of a triangular lattice of equivalent adsorption sites using the conventional canonical ensemble MC simulation method with Metropolis sampling.[22a,c,29] To eliminate edge effects, we used periodic boundary conditions in both planar directions. Molecule **1** was modeled as a rigid C_3-symmetric tripod built of four discrete segments, each of which occupies one site on a triangular lattice.[22a,c,29] In the approach adopted here, the core segment of the tripod corresponds to the central phenyl ring of **1**, while the three single-membered arms represent the outer pyridyl groups. The adsorbed molecules were allowed to interact via a short-range interaction potential limited to the nearest neighbors on a triangular lattice. Solvent molecules were neglected.

STM Investigation. STM measurements were performed using a Veeco scanning tunneling microscope (multimode Nanoscope III, Veeco) at the interface between a highly oriented pyrolitic graphite (HOPG) substrate and a supernatant solution, thereby mapping a maximum area of 1×1 μm. Solutions of **1** were applied to the basal plane of the surface. For STM measurements, the substrates were glued to a magnetic disk, and an electric contact was made with silver paint (Aldrich Chemicals). The STM tips were mechanically cut from a Pt/Ir wire (90/10, diameter 0.25 mm). The raw STM data were processed through the application of background flattening, and the drift was corrected using the

dx.doi.org/10.1021/ja4002025 | J. Am. Chem. Soc. 2013, 135, 6942−6950

underlying graphite lattice as a reference. The lattice was visualized by lowering the bias voltage to 20 mV and raising the current up to 65 pA. A mother solution of **1** was dissolved in chloroform and diluted with 1-phenyloctane to give 200, 20, and 2 μM solutions. STM imaging was carried out in constant height mode without turning off the feedback loop, to avoid tip crashes. Monolayer pattern formation was achieved by applying onto freshly cleaved HOPG 4 μL of a solution that was previously heated at 60−70 °C for 1 h to improve the solubility and dissolve any aggregates. The STM images were recorded at room temperature once achieving a negligible thermal drift. All of the molecular models were minimized with Chem3D at the MM2 level and processed with QuteMol[30] visualization software.

RESULTS AND DISCUSSION

Theoretical Studies. Initially N molecules of **1** were randomly distributed on the 2D lattice. The adsorbate density, ρ, was defined as the average number of segments per single lattice site, i.e., 4 NL^{-2}, since single molecule **1** is composed of 4 segments. To equilibrate the system at temperature T, a sequence of trial MC moves was performed. To this end, one of the adsorbed molecules was selected at random, and its potential energy in an initial configuration (U_{old}) was calculated. This procedure involved identification of all the bimolecular clusters to which the selected molecule belonged and subsequent summation of the associated energies U_x (see Figure 1). Once U_{old} was calculated, an attempt was made to translate the molecule to a new, randomly chosen position on the 2D lattice. To move the molecule over the surface, a cluster of four adjacent adsorption sites matching the shape of the molecule was chosen at random. If none of the selected cluster sites were occupied, the interaction energy, U_{new}, of the new configuration was calculated using the same method as for U_{old}. To decide if the move was successful, the acceptance probability, P_{acc}, was calculated (eq 2) and compared with a randomly generated number $r \in (0,1)$:

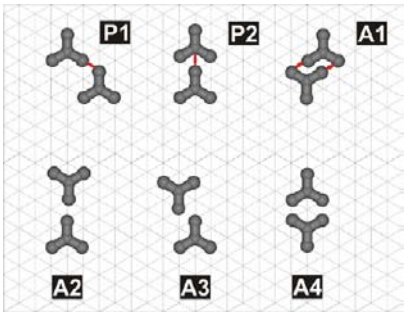

Figure 1. Six possible configurations of a pair of neighboring molecules of **1** forming a dimer adsorbed on a triangular lattice. The letter codes correspond to the parallel (P) and antiparallel (A) relative orientation of the molecules. Mirror images of P1 and A3 are omitted for clarity. The red thick lines represent intermolecular N···H−C bonds formed within $\mathbf{1}_2$P1, $\mathbf{1}_2$P2, and $\mathbf{1}_2$A1 dimers.

$$P_{acc} = \min(1, e^{\Delta U/kT}) \quad (2)$$

and

$$\Delta U = U_{new} - U_{old}$$

with k being the Boltzmann constant.

If $R < P_{acc}$, then the molecule was moved to the new position, otherwise it remained in its initial place. The above sequence was repeated for each adsorbed molecule, constituting one MC step. To equilibrate the system, we used up to 10^8 MC steps. The net interaction energy of a pair of neighboring molecules (U_x) was dependent on their relative configuration, x, which in our case correlated to one of six possible orientations, shown schematically in Figure 1.

Figure 1 reveals that only configurations P1, P2, and A1 allow for the formation of N−H bonds. In the remaining cases, the molecules are oriented in such a way that either two nitrogen atoms (A2) or two hydrogen atoms (A3 and A4) are in closest contact, obviating H-bonding. To elucidate the role of H-bonding on the stabilization of the physisorbed monolayer for configurations P1, P2, and A1, DFT calculations of the potential interaction energies of the molecular dimers depicted in Figure 1 were carried out. In particular, three dimeric forms of **1**, i.e. $\mathbf{1}_2$P1, $\mathbf{1}_2$P2, and $\mathbf{1}_2$A1 (Figure 2a−c), were minimized by using B3LYP/6-311G(d,p) basis set, and the strengths of the H-bonds were evaluated to facilitate a comparison between the three possible structures (not minimized) (Figure 2d−f) and experimental molecular packing in 2D on a solid surface investigated by STM (*vide infra*). From these calculations it was predicted that the $\mathbf{1}_2$A1 dimer contains two H-bonds between its substituent molecules, in contrast to the single H-bonds found in the $\mathbf{1}_2$P1 and $\mathbf{1}_2$P2 dimers (Figure 2, blue). These interactions were normalized to give a single H-bond energies of E_{P1} = 6.32 kJ mol^{-1}, E_{P2} = 5.78 kJ mol^{-1}, and E_{A1} = 3.31 kJ mol^{-1}. Due to the presence of multiple repulsive interactions and the absence of H-bonding, the dimeric structures $\mathbf{1}_2$A2, $\mathbf{1}_2$A3, and $\mathbf{1}_2$A4 were unstable during DFT simulations.

To simplify the parameters contained in our MC model, the apparent instability of **A2**, **A3**, and **A4** dimers as revealed by DFT studies prompted the assumption that $E_{A2} = E_{A3} = E_{A4} = 0$. The stabilized arrays, shown in Figure 2d−f, were used to furnish infinite defect-free layer energies of 18.96 kJ mol^{-1} for $\mathbf{1}_n$P1, 17.34 kJ mol^{-1} for $\mathbf{1}_n$P2, and 9.91 kJ mol^{-1} for $\mathbf{1}_n$A1.

Figure 3 displays the effect of the density of the adsorbed overlayer (ρ) on the formation of ordered phases comprising molecules **1**. With decreasing ρ values, the high-density phase $\mathbf{1}_n$P2 (red) is gradually displaced by the low-density phase $\mathbf{1}_n$P1 (blue). The calculated densities of these phases are 1 and 4/7, respectively.

Figure 4 portrays snapshots of the physisorbed phase with ρ = 0.57 (corresponding to 4/7) and T = 295.15 K, during the MC equilibration. This process is further illustrated in Figure 5, which shows changes in the mean potential energy of the adlayer with points (a−f) corresponding to the six snapshots from Figure 4. The energy increases gradually from 7.14 kJ mol^{-1} (random starting configuration) up to 18.93 kJ mol^{-1}, which corresponds to the formation of the ordered phase $\mathbf{1}_n$P1 that fills the entire lattice. At the early stage of the equilibration the adsorbed configuration (a) is characterized by a relatively low potential energy, as it comprises a large number of small domains, mostly of $\mathbf{1}_n$P1 type. Existence of such small $\mathbf{1}_n$P1 domains is unfavorable because of high energetic cost associated with the undercoordinated peripheral molecules of **1**. The gradual increase of the energy shown in Figure 5 means the formation of new $\mathbf{1}_2$P1 configurations and coalescence of the domains. The two remaining configurations $\mathbf{1}_2$A1 and $\mathbf{1}_2$P1 are also present in the adlayer, but their contribution vanishes as the simulation proceeds. This is confirmed by the energy at equilibrium (plateau at 18.96 kJ mol^{-1}), which clearly

dx.doi.org/10.1021/ja4002025 | J. Am. Chem. Soc. 2013, 135, 6942−6950

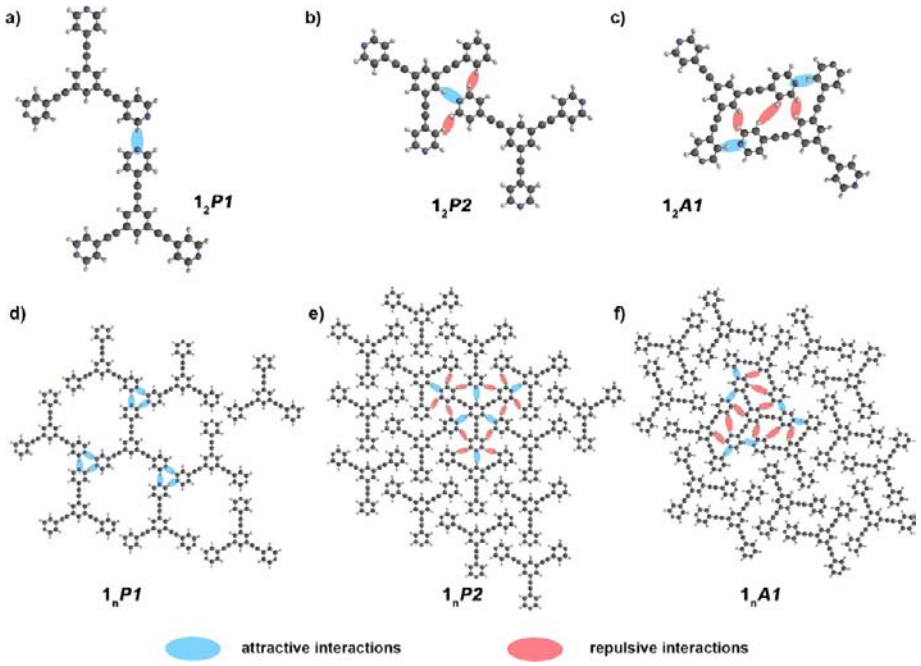

Figure 2. Schematic representation of computed H-bonded dimers: (a) $\mathbf{1}_2$P1, (b) $\mathbf{1}_2$P2, and (c) $\mathbf{1}_2$A1 modeled with DFT. Supramolecular 2D arrays of **1** corresponding to the motifs (not minimized): (d) $\mathbf{1}_n$P1, (e) $\mathbf{1}_n$P2, and (f) $\mathbf{1}_n$A1.

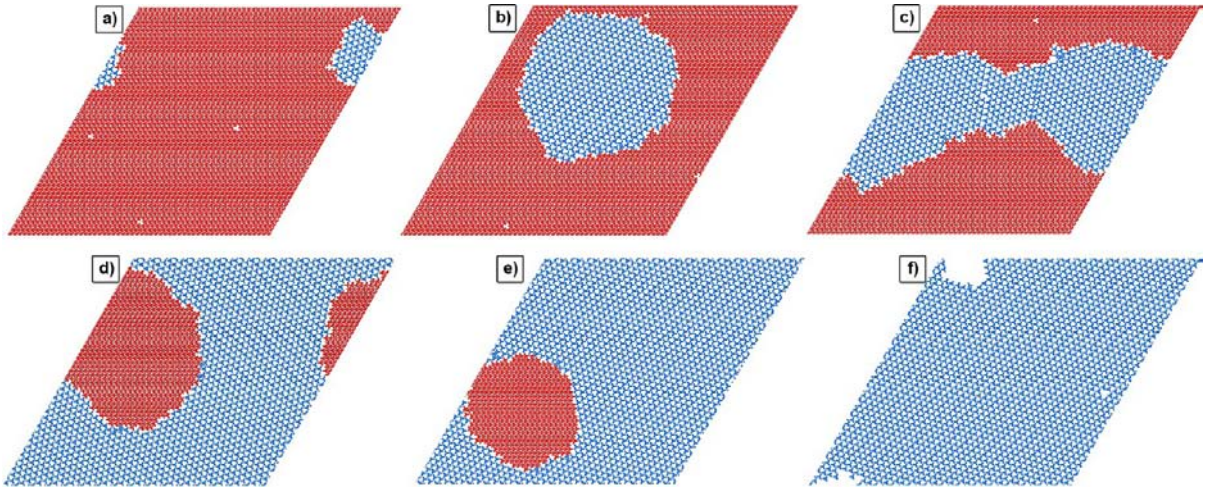

Figure 3. Progression of ordered phases observed for the systems comprising (a) 3060, (b) 2713, (c) 2520, (d) 2150, (e) 2000, and (f) 1750 molecules of **1** adsorbed on a 112 × 112 triangular lattice at T = 295.15 K. The snapshots show equilibrium configurations for which the density of the adsorbed phase, ρ, equals (a) 0.98, (b) 0.86, (c) 0.80, (d) 0.69, (e) 0.64, and (f) 0.56 (rounded values). The areas colored in red and blue correspond to the ordered phases $\mathbf{1}_n$P2 and $\mathbf{1}_n$P1, respectively.

demonstrates that $\mathbf{1}_n$P1 is the preferred structure for the assumed ρ and T.

We emphasize that the evolution of the structure of the adsorbed phase shown in Figure 4 is not related to real time, since in the equilibrium MC simulation technique, there is by definition no direct correspondence between MC steps and a real time unit. The main purpose of the figure is to demonstrate how the structure evolves from the initial disordered (inequilibrium) state to the final (equilibrium) extended ordered pattern. For a dynamic visualization of the $\mathbf{1}_n$P1 phase formation see the Supporting Information (movie), which contains 33 snapshots taken along the energy curve.

To determine the effect of solute concentration on the phase behavior in our system, we performed additional MC calculations using the conventional grand canonical MC (GCMC) simulation method.[29] These simulations were executed on a 56 × 56 triangular lattice at T = 295.15 and 343.15 K. In this case, the surface was an open system in contact with the bulk phase with a fixed chemical potential for molecule **1**, μ. To mimic the experimental procedure, each simulation run at a given value of μ was initiated from an empty surface. The system was equilibrated using a sequence of MC steps, each of which involved the random insertion, deletion, or translation of a molecule with a probability defined according to the standard Metropolis GCMC scheme.[29] To reach the equilibrium state, we used 10^8 steps per one lattice site. Since for the diluted solutions used here μ is proportional to the logarithm of the solute concentration, the changes in μ fully reflect the corresponding changes in concentration, enabling qualitative analysis of the effect of concentration on the phase

dx.doi.org/10.1021/ja4002025 | J. Am. Chem. Soc. 2013, 135, 6942−6950

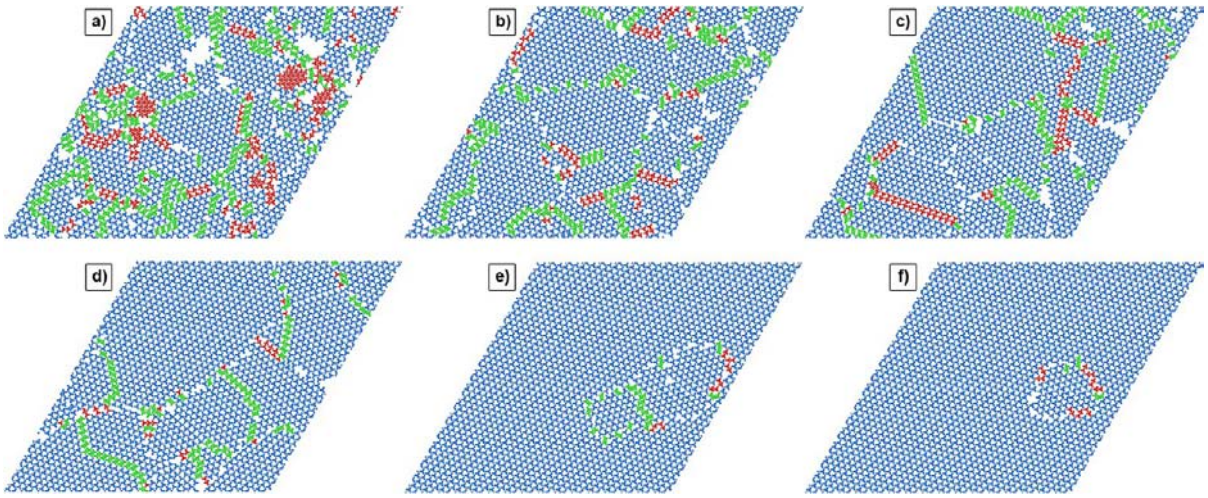

Figure 4. Evolution of the structure of the adsorbed phase during one MC simulation performed for the system comprising 1787 molecules of **1** adsorbed on a 112 × 112 lattice (ρ = 0.57) at T = 295.15 K. The molecules represented in red, green, and blue correspond to $\mathbf{1}_n$P2, $\mathbf{1}_n$A1, $\mathbf{1}_n$P1 phases, respectively.

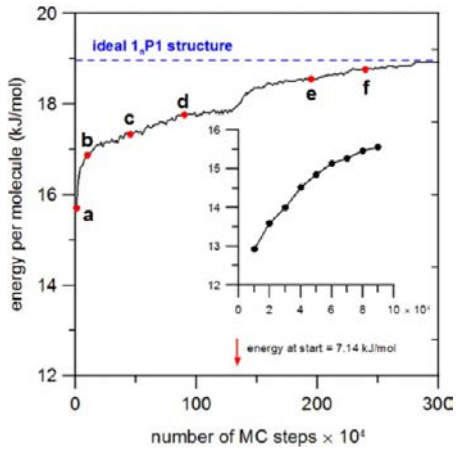

Figure 5. Changes in the mean potential energy per molecule during one MC run obtained for a system comprising 1787 molecules of **1** adsorbed on a 112 × 112 lattice (ρ = 0.57) at T = 295.15 K. The red points marked (a–f) are the energies of the corresponding adsorbed configurations shown in Figure 4. The insert shows the initial increase of the energy observed within the first 10^4 MC steps. The blue dashed line corresponds to the mean potential energy of molecule **1** in an infinite defect-free structure $\mathbf{1}_n$P1, i.e., 18.96 kJ mol^{-1}.

coexistence in the adsorbed overlayer (see the Supporting Information, Part A). Figure 6 shows the results of the simulations averaged over 10 independent runs, revealing that at 295.15 K, the first phase transformation, from 2D lattice gas to the ordered pattern $\mathbf{1}_n$P1, occurs at $\mu \approx -12.40$ kJ mol^{-1}. The pattern $\mathbf{1}_n$P1 having a rhombic unit cell with side equal to $\sqrt{7}$ (Figure 6) and ρ = 4/7 (0.57) dominates the system as long as the chemical potential does not exceed ca. −9.40 kJ mol^{-1}. At this point, another phase change occurs, leading to the formation of the closely packed pattern $\mathbf{1}_n$P2 with rhombic unit cell of side 2 and ρ = 1. At the elevated temperature 343.15 K, the qualitative effect of μ on the phase behavior is similar, but the entire curve (dashed line) shifts toward higher chemical potential values. To induce the phase transformation from $\mathbf{1}_n$P1 to $\mathbf{1}_2$P1, a more concentrated solution has to be used. The observed phase progression induced by the increase of the chemical potential (solute concentration) is consistent with experimental observations (*vide infra*).

To validate further ability of the proposed theoretical approach to reproduce phase coexistence in other physisorbed overlayers stabilized by H-bonds, we performed additional simulations of the self-assembly of the partially fluorinated tripod-shaped molecule **2** (Figure 7) at the phenyloctane–HOPG interface, which has been studied experimentally by Mu and co-workers.[31] In that system the crucial stabilizing role is played by the aryl–H···F H-bonds, which allow the formation of extended chiral honeycomb structure with hexagonal void spaces. To explore the effect of surface coverage on the morphology of the adlayer comprising the fluorinated building blocks, we used the same procedure as for **1**. Details of DFT calculations and MC modeling are provided in the Supporting Information (Part B).

The results of the simulations performed for molecule **2** demonstrate the initial formation of the hexagonal $\mathbf{2}_n$AF1 pattern (orange) with a rhombic unit cell with sides equal to $\sqrt{21}$ and ρ = 2/3 (0.67). The structure of the predicted porous adlayer agrees well with the experiment, and it remains stable until the density of the adsorbed phase is lower than 2/3, that is also at submonolayer coverage with respect to $\mathbf{2}_n$AF1 (see Figure S4, Part C). With increasing ρ values, the low-density phase $\mathbf{2}_n$AF1 is gradually displaced by the high-density linear phase $\mathbf{2}_n$PF1 (purple) with a rectangular $3 \times 3\sqrt{3}$ unit cell and ρ = 7/9 (0.78).

STM. STM was used to probe the self-assembly behavior of molecule **1** at solution–graphite interfaces. Initially, we investigated the self-assembled structures by applying a drop of a 200 ± 2 μM solution of **1** in 1-phenyloctane on the graphite surface. Figure 8a,b shows STM height images (i.e., recorded in constant-current mode) of the obtained physisorbed monolayer, revealing a polycrystalline structure consisting of crystalline domains of hundreds of square nanometers. These domains, which are stable for 3–4 h, exhibit a unit cell: $a = b$ = (1.33 ± 0.02) nm, α = (60 ± 2)°, leading to an area A = (1.51 ± 0.04) nm^2, with each unit cell containing a single molecule **1**. The supramolecular structure can be well described by the formation of six weak N(pyridyl)···H–C(aryl) H-bonds per molecule, wherein molecules adopt a P2 configuration. The formation of such

dx.doi.org/10.1021/ja4002025 | J. Am. Chem. Soc. 2013, 135, 6942–6950

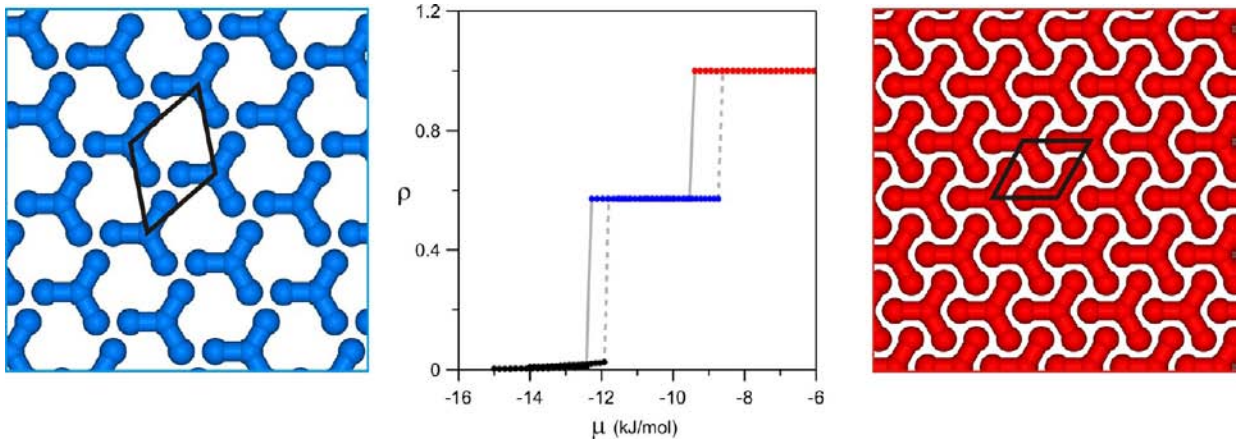

Figure 6. Dependence of the density of the physisorbed layer on the chemical potential of molecule **1** in the bulk phase (center) averaged from 10 simulations on a 56 × 56 triangular lattice at T = 295.15 and 343.15 K (solid and dashed lines, respectively). The ordered patterns shown in red (right) and blue (left) correspond to the molecular configurations present at the intervals of μ marked by the corresponding color.

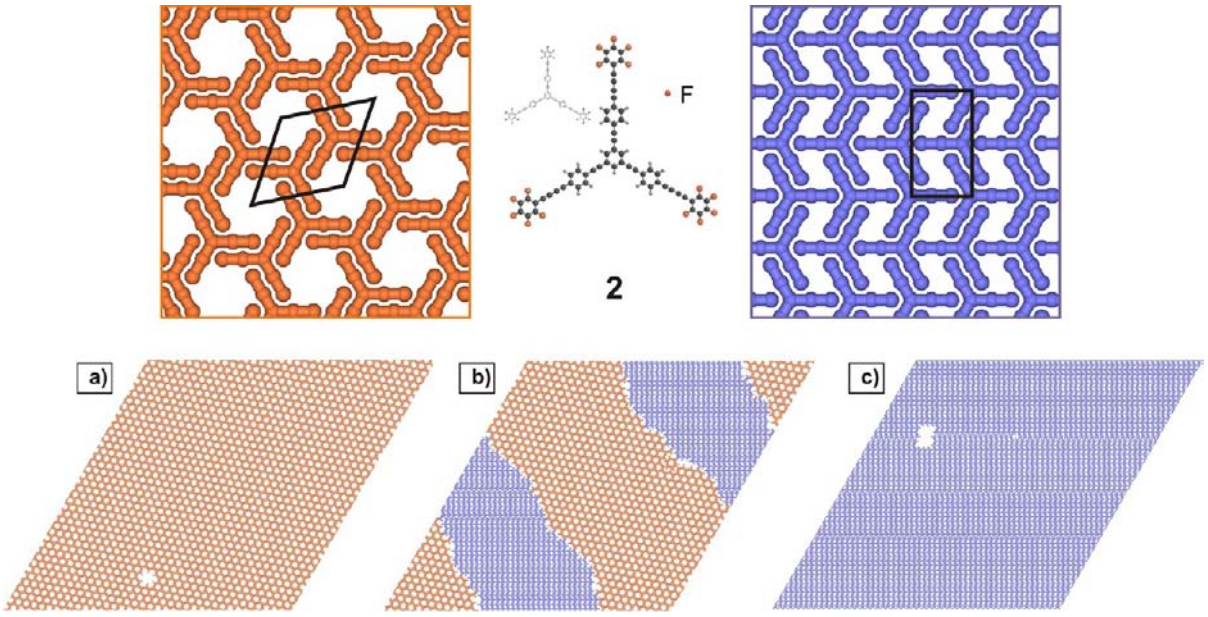

Figure 7. Progression of ordered phases observed for the systems comprising (a) 2682, (b) 2823, and (c) 3121 molecules of **2** (top center) adsorbed on a 168 × 168 triangular lattice at T = 295.15 K. The snapshots show equilibrium configurations for which the density of the adsorbed phase, ρ, equals (a) 0.66, (b) 0.70, and (c) 0.77 (rounded values). The areas colored in orange and purple correspond to the ordered phases $\mathbf{2}_n$AF1 and $\mathbf{2}_n$PF1, respectively, whose magnified fragments are shown in the top part.

densely packed 2D architectures is in agreement with the $\mathbf{1}_n$P2 structure computed at high concentrations of **1** (see Figure 3a). Importantly, similar structures were observed when a drop of 150, 100, and 50 μM solutions were applied to the HOPG surface.

As revealed by MC simulations, the formation of submonolayer-thick films of **1** at different concentrations can lead to the generation of different supramolecular motifs; because of this, we extended our experimental studies to films prepared from highly diluted (20 ± 1 μM) solutions. STM imaging of these films revealed the generation of 2D porous crystalline domains (Figure 8d,e). These porous domains exhibit a unit cell $a = b = (1.62 \pm 0.02)$ nm, $\alpha = (63 \pm 2)°$, leading to an area $A = (2.34 \pm 0.04)$ nm^2, with each unit cell containing a single molecule of **1**. By linking those experimental results with theoretical calculations, we could conclude that the supramolecular porous structure can be well described by the formation of six weak N(pyridyl)···H−C(pyridyl) H-bonds per molecule in the right-handed fashion (see red arrow in Figure 8f), where a P1 configuration is adopted. Such a 2D porous architecture is in agreement with the $\mathbf{1}_n$P1 motif computed at low concentration of **1** (see Figure 3f). The nonchiral character of the graphite substrate, as well as the absence of chiral centers in the structure of investigated molecules, should result in **1** self-assembling into a racemic mixture, physisorbed on the surface. That is, left- and right-handed structures should be observed with each configuration appearing in equal proportions. However, only one large crystalline domain featuring a single chirality was monitored on the surface by STM. These results have been obtained using an A scanner (Veeco), therefore mapping an area of with a maximum size of 1 × 1 μm. Despite several additional experiments that were carried out using solutions with concentrations ranging from 20 ± 1 down to 5 ± 1 μM in order to explore the potential

dx.doi.org/10.1021/ja4002025 | J. Am. Chem. Soc. 2013, 135, 6942−6950

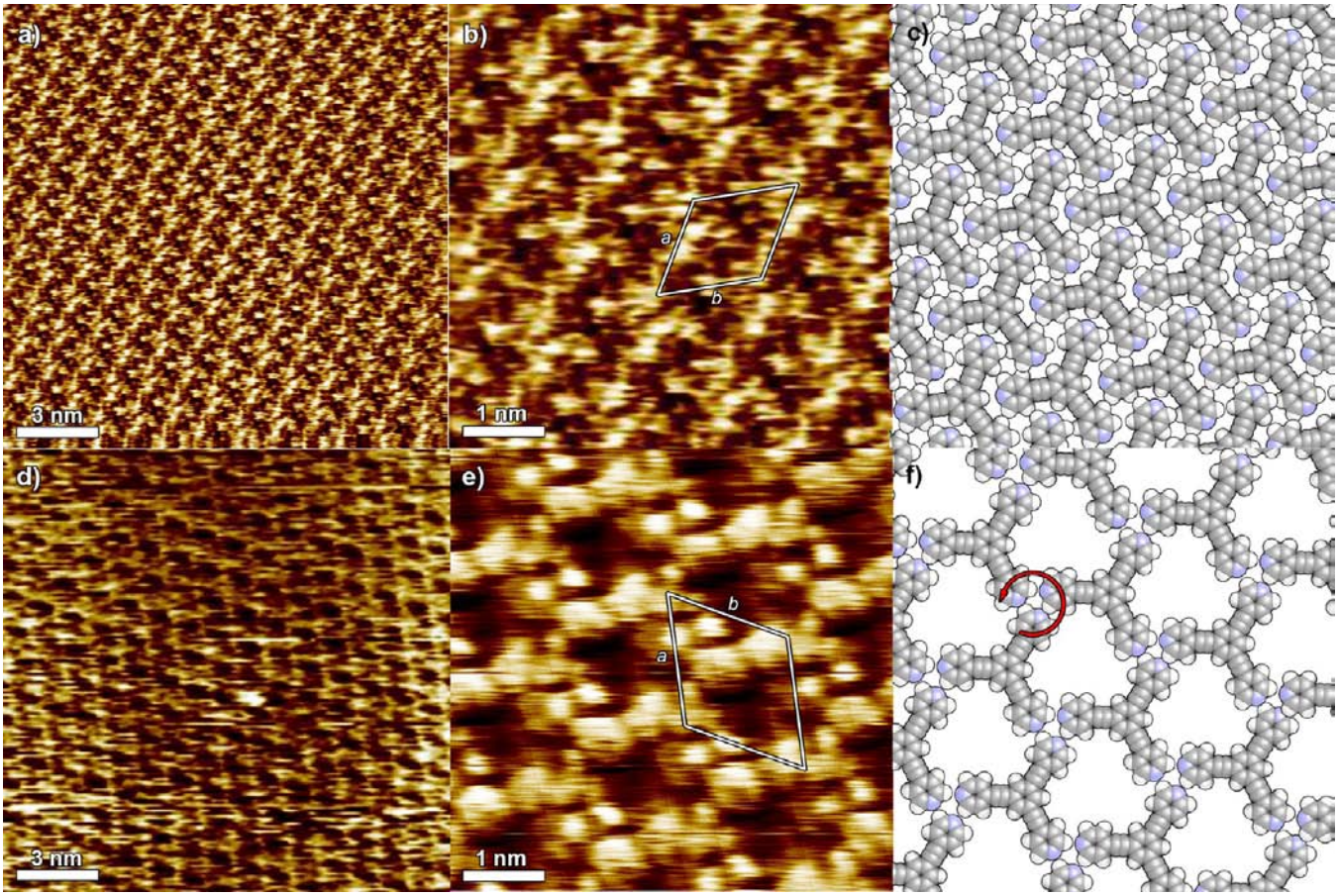

Figure 8. (a) and (b) STM height images of a $\mathbf{1}_n$P2 supramolecular structure at the solid–liquid interface, self-assembled from a solution of **1** in 1-phenyloctane. (c) Schematic representation of the $\mathbf{1}_n$P2 array. (d) and (e) STM height images of a $\mathbf{1}_n$P1 supramolecular porous network at the solid–liquid interface. (f) Schematic representation of the $\mathbf{1}_n$P1 network, the red arrow indicates the chiral nature of weak H-bonds. Tunneling parameters: average tunneling current (I_t) = 15 pA, tip bias voltage (V_t) = (a,b) 300 and (c,d) 350 mV.

coexistence of left- and right-hand domains, such a phenomenon was never observed. Numerous additional experiments were carried out using solutions with concentrations spanning from 50 to 22 μM in order to study the potential coexistence of $\mathbf{1}_n$P2 arrays and $\mathbf{1}_n$P1 2D porous architectures. Yet, one type of structure, $\mathbf{1}_n$P2, was exclusively observed, confirming that porous architectures are formed on HOPG surfaces only when solutions of **1** with concentrations $\lesssim$20 μM are used.

Noteworthy, only two supramolecular structures, i.e. $\mathbf{1}_n$P1 and $\mathbf{1}_n$P2, have been observed at the solid–liquid interface, highlighting the importance of the strength of intermolecular interactions. As shown by MC simulations, the average interaction energies in defect-free layers of porous structure $\mathbf{1}_n$P1 (18.96 kJ mol^{-1}) and densely packed $\mathbf{1}_n$P2 network (17.34 kJ mol^{-1}) are much stronger than those in $\mathbf{1}_n$A1 assembly (9.91 kJ mol^{-1}), therefore its existence at the solid–liquid interface is energetically unfavorable.

CONCLUSIONS

In summary, we demonstrated that complex 2D molecular architectures on solid surfaces can be effectively modeled using simple theoretical tools, such as the lattice gas MC method, which takes into account only nearest-neighbor intermolecular interactions. We have shown both experimentally by STM imaging at the solid–liquid interface and by MC calculations that the self-assembly behavior of **1** molecules on HOPG is concentration dependent, forming either densely packed $\mathbf{1}_n$P2 arrays or porous $\mathbf{1}_n$P1 structures at high (200–20 μM) or low (20–5 μM) concentrations, respectively. In particular, STM studies confirmed that upon the use of relatively high concentrations of **1**, $\mathbf{1}_n$P2 2D arrays are formed, characterized by the presence of weak N(pyridyl)···H–C(aryl) H-bonds. Conversely, upon the use of low concentrations of **1**, a 2D supramolecular porous network featuring a $\mathbf{1}_n$P1 motif is formed, characterized by chelical N(pyridyl)···H–C(pyridyl) H-bonding. Each self-assembly motif was found to be an energetic minimum, and transition phases between the two arrays were not observed over the course of STM imaging. The computational approach devised in this paper can be used for predicting concentration-dependent molecular self-assembly in 2D on solid surfaces. The ability to predict the concentration regimes for which a given 2D array will be formed for a given substrate is extremely useful when targeting a particular architecture, obviating the need for material-intensive experimental trials at a myriad of concentrations. These methods will aid in the rational design of 2D arrays which form with weak, noncovalent bonding as the impetus. While the model system used here relies on H-bonding, this approach lays the foundation for computational investigations for any systems in which weak, intermolecular interactions can be evaluated.

dx.doi.org/10.1021/ja4002025 | J. Am. Chem. Soc. 2013, 135, 6942–6950

■ ASSOCIATED CONTENT

Supporting Information

Dynamic visualization of the $\mathbf{1}_n$P1 phase formation, which shows 33 snapshots taken along the energy curve. Details of analysis of the effect of concentration on the phase coexistence in the adsorbed overlayer of **1**. MC simulation details for 1,3,5-tris(pyridine-4-ylethynyl)benzene (**2**). This material is available free of charge via the Internet at http://pubs.acs.org.

■ AUTHOR INFORMATION

Corresponding Author

szabla@vega.umcs.lublin.pl; stang@chem.utah.edu; samori@unistra.fr

Notes

The authors declare no competing financial interest.

■ ACKNOWLEDGMENTS

We thank Dr. Marco Cecchini for fruitful discussions. This work was financially supported by ERC project SUPRA-FUNCTION (GA-257305), the International Center for Frontier Research in Chemistry (icFRC). P.J.S. thanks the NSF (grant 1212799) for financial support.

■ REFERENCES

(1) (a) Whitesides, G. M.; Mathias, J. P.; Seto, C. T. *Science* **1991**, *254*, 1312. (b) Lehn, J.-M. *Science* **1993**, *260*, 1762. (c) Breault, G. A.; Hunter, C. A.; Mayers, P. C. *Tetrahedron* **1999**, *55*, 5265. (d) van Esch, J. H.; Feringa, B. L. *Angew. Chem., Int. Ed.* **2000**, *39*, 2263. (e) Fenniri, H.; Deng, B. L.; Ribbe, A. E. *J. Am. Chem. Soc.* **2002**, *124*, 11064. (f) Elemans, J. A. A. W.; Rowan, A. E.; Nolte, R. J. M. *J. Mater. Chem.* **2003**, *13*, 2661. (g) Hoeben, F. J. M.; Jonkheijm, P.; Meijer, E. W.; Schenning, A. P. H. J. *Chem. Rev.* **2005**, *105*, 1491. (h) Palermo, V.; Samorì, P. *Angew. Chem., Int. Ed.* **2007**, *46*, 4428. (i) Palmer, L. C.; Stupp, S. I. *Acc. Chem. Res.* **2008**, *41*, 1674. (j) Li, Q. W.; Zhang, W. Y.; Miljanic, O. S.; Sue, C. H.; Zhao, Y. L.; Liu, L. H.; Knobler, C. B.; Stoddart, J. F.; Yaghi, O. M. *Science* **2009**, *325*, 855.

(2) (a) De Feyter, S.; De Schryver, F. C. *Chem. Soc. Rev.* **2003**, *32*, 139. (b) Barth, J. V.; Costantini, G.; Kern, K. *Nature* **2005**, *437*, 671. (c) Elemans, J. A. A. W.; Lei, S. B.; De Feyter, S. *Angew. Chem., Int. Ed.* **2009**, *48*, 7298. (d) Ciesielski, A.; Palma, C. A.; Bonini, M.; Samorì, P. *Adv. Mater.* **2010**, *22*, 3506.

(3) (a) Elemans, J. A. A. W.; Van Hameren, R.; Nolte, R. J. M.; Rowan, A. E. *Adv. Mater.* **2006**, *18*, 1251. (b) Surin, M.; Samorì, P.; Jouaiti, A.; Kyritsakas, N.; Hosseini, M. W. *Angew. Chem., Int. Ed.* **2007**, *46*, 245. (c) Spada, G. P.; Lena, S.; Masiero, S.; Pieraccini, S.; Surin, M.; Samorì, P. *Adv. Mater.* **2008**, *20*, 2433. (d) Ciesielski, A.; Piot, L.; Samorì, P.; Jouaiti, A.; Hosseini, M. W. *Adv. Mater.* **2009**, *21*, 1131. (e) Kudernac, T.; Lei, S. B.; Elemans, J. A. A. W.; De Feyter, S. *Chem. Soc. Rev.* **2009**, *38*, 402. (f) Ciesielski, A.; Lena, S.; Masiero, S.; Spada, G. P.; Samorì, P. *Angew. Chem., Int. Ed.* **2010**, *49*, 1963.

(4) DiBenedetto, S. A.; Facchetti, A.; Ratner, M. A.; Marks, T. J. *Adv. Mater.* **2009**, *21*, 1407.

(5) (a) Samorì, P.; Müllen, K.; Rabe, H. P. *Adv. Mater.* **2004**, *16*, 1761. (b) Cordier, P.; Tournilhac, F.; Soulie-Ziakovic, C.; Leibler, L. *Nature* **2008**, *451*, 977.

(6) (a) Gomar-Nadal, E.; Abdel-Mottaleb, M. M. S.; De Feyter, S.; Veciana, J.; Rovira, C.; Amabilino, D. B.; De Schryver, F. C. *Chem.Commun.* **2003**, 906. (b) Jackson, A. M.; Myerson, J. W.; Stellacci, F. *Nat. Mater.* **2004**, *3*, 330. (c) Lei, S.; Puigmarti-Luis, J.; Minoia, A.; Van der Auweraer, M.; Rovira, C.; Lazzaroni, R.; Amabilino, D. B.; De Feyter, S. *Chem. Commun.* **2008**, 703. (d) Centrone, A.; Penzo, E.; Sharma, M.; Myerson, J. W.; Jackson, A. M.; Marzari, N.; Stellacci, F. *Proc. Natl. Acad. Sci. U.S.A.* **2008**, *105*, 9886. (e) Ciesielski, A.; Palma, C.-A.; Bonini, M.; Samorì, P. *Adv. Mater.* **2010**, *22*, 3506. (f) Mohnani, S.; Bonifazi, D. *Coord. Chem. Rev.* **2010**, *254*, 2342.

(7) (a) Barth, J. V. *Annu. Rev. Phys. Chem.* **2007**, *58*, 375. (b) Kühnle, A. *Curr. Opin. Colloid Interface Sci.* **2009**, *14*, 157.

(8) Katsonis, N.; Lacaze, E.; Feringa, B. L. *J. Mater. Chem.* **2008**, *18*, 2065.

(9) Piot, L.; Bonifazi, D.; Samorì, P. *Adv. Funct. Mater.* **2007**, *17*, 3689.

(10) (a) Nath, K. G.; Ivasenko, O.; MacLeod, J. M.; Miwa, J. A.; Wuest, J. D.; Nanci, A.; Perepichka, D. F.; Rosei, F. *J. Phys. Chem. C* **2007**, *111*, 16996. (b) Cicoira, F.; Santano, C.; Rosei, F. *Top. Curr. Chem.* **2008**, *285*, 203. (c) Furukawa, S.; De Feyter, S. *Top. Curr. Chem.* **2008**, *287*, 87. (d) Tahara, K.; Okuhata, S.; Adisoejoso, J.; Lei, S. B.; Fujita, T.; De Feyter, S.; Tobe, Y. *J. Am. Chem. Soc.* **2009**, *131*, 17583.

(11) (a) Dmitriev, A.; Lin, N.; Weckesser, J.; Barth, J. V.; Kern, K. *J. Phys. Chem. B* **2002**, *106*, 6907. (b) Theobald, J. A.; Oxtoby, N. S.; Phillips, M. A.; Champness, N. R.; Beton, P. H. *Nature* **2003**, *424*, 1029. (c) Griessl, S. J. H.; Lackinger, M.; Jamitzky, F.; Markert, T.; Hietschold, M.; Heckl, W. A. *Langmuir* **2004**, *20*, 9403. (d) Yan, H. J.; Lu, J.; Wan, L. J.; Bai, C. L. *J. Phys. Chem. B* **2004**, *108*, 11251. (e) Stöhr, M.; Wahl, M.; Galka, C. H.; Riehm, T.; Jung, T. A.; Gade, L. H. *Angew. Chem., Int. Ed.* **2005**, *44*, 7394. (f) MacLeod, J. M.; Ivasenko, O.; Perepichka, D. F.; Rosei, F. *Nanotechnology* **2007**, *18*, 3347. (g) Blunt, M. O.; Russell, J. C.; Gimenez-Lopez, M. D.; Garrahan, J. P.; Lin, X.; Schroder, M.; Champness, N. R.; Beton, P. H. *Science* **2008**, *322*, 1077. (h) Blunt, M.; Lin, X.; Gimenez-Lopez, M. D.; Schroder, M.; Champness, N. R.; Beton, P. H. *Chem.Commun.* **2008**, 2304. (i) Madueno, R.; Räisänen, M. T.; Silien, C.; Buck, M. *Nature* **2008**, *454*, 618. (j) Zhang, X.; Chen, T.; Yan, H. J.; Wang, D.; Fan, Q. H.; Wan, L. J.; Ghosh, K.; Yang, H. B.; Stang, P. J. *Acs Nano* **2010**, *4*, 5685. (k) Ciesielski, A.; Cadeddu, A.; Palma, C. A.; Gorczynski, A.; Patroniak, V.; Cecchini, M.; Samorì, P. *Nanoscale* **2011**, *3*, 4125. (l) Fu, C. Y.; Rosei, F.; Perepichka, D. F. *ACS Nano* **2012**, *6*, 7973.

(12) (a) Spillmann, H.; Dmitriev, A.; Lin, N.; Messina, P.; Barth, J. V.; Kern, K. *J. Am. Chem. Soc.* **2003**, *125*, 10725. (b) Dmitriev, A.; Spillmann, H.; Lin, N.; Barth, J. V.; Kern, K. *Angew. Chem., Int. Ed.* **2003**, *42*, 2670. (c) Stepanow, S.; Lingenfelder, M.; Dmitriev, A.; Spillmann, H.; Delvigne, E.; Lin, N.; Deng, X. B.; Cai, C. Z.; Barth, J. V.; Kern, K. *Nat. Mater.* **2004**, *3*, 229. (d) Klappenberger, F.; Kuhne, D.; Krenner, W.; Silanes, I.; Arnau, A.; de Abajo, F. J. G.; Klyatskaya, S.; Ruben, M.; Barth, J. V. *Nano Lett.* **2009**, *9*, 3509. (e) Kühne, D.; Klappenberger, F.; Decker, R.; Schlickum, U.; Brune, H.; Klyatskaya, S.; Ruben, M.; Barth, J. V. *J. Am. Chem. Soc.* **2009**, *131*, 3881.

(13) (a) Charra, F.; Cousty, J. *Phys. Rev. Lett.* **1998**, *80*, 1682. (b) Samorì, P.; Fechtenkotter, A.; Jäckel, F.; Böhme, T.; Müllen, K.; Rabe, J. P. *J. Am. Chem. Soc.* **2001**, *123*, 11462. (c) Tahara, K.; Furukawa, S.; Uji-I, H.; Uchino, T.; Ichikawa, T.; Zhang, J.; Mamdouh, W.; Sonoda, M.; De Schryver, F. C.; De Feyter, S.; Tobe, Y. *J. Am. Chem. Soc.* **2006**, *128*, 16613. (d) Bléger, D.; Kreher, D.; Mathevet, F.; Attias, A. J.; Schull, G.; Huard, A.; Douillard, L.; Fiorini-Debuischert, C.; Charra, F. *Angew. Chem., Int. Ed.* **2007**, *46*, 7404. (e) Elemans, J. A. A. W.; De Cat, I.; Xu, H.; De Feyter, S. *Chem. Soc. Rev.* **2009**, *38*, 722. (f) Adisoejoso, J.; Tahara, K.; Okuhata, S.; Lei, S.; Tobe, Y.; De Feyter, S. *Angew. Chem., Int. Ed.* **2009**, *48*, 7353. (g) Bonini, M.; Zalewski, L.; Breiner, T.; Dotz, F.; Kastler, M.; Schadler, V.; Surin, M.; Lazzaroni, R.; Samorì, P. *Small* **2009**, *5*, 1521. (h) Chen, T.; Pan, G. B.; Wettach, H.; Fritzsche, M.; Hoger, S.; Wan, L. J.; Yang, H. B.; Northrop, B. H.; Stang, P. J. *J. Am. Chem. Soc.* **2010**, *132*, 1328.

(14) (a) Sherrington, D. C.; Taskinen, K. A. *Chem. Soc. Rev.* **2001**, *30*, 83. (b) Desiraju, G. R. *Acc. Chem. Res.* **2002**, *35*, 565.

(15) (a) Macdonald, J. C.; Whitesides, G. M. *Chem. Rev.* **1994**, *94*, 2383. (b) Palma, C.-A.; Björk, J.; Bonini, M.; Dyer, M. S.; Llanes-Pallas, A.; Bonifazi, D.; Persson, M.; Samorì, P. *J. Am. Chem. Soc.* **2009**, *131*, 13062. (c) Palma, C.-A.; Bonini, M.; Llanes-Pallas, A.; Breiner, T.; Prato, M.; Bonifazi, D.; Samorì, P. *Chem. Commun.* **2008**, 5289.

(16) (a) Meier, C.; Ziener, U.; Landfester, K.; Weihrich, P. *J. Phys. Chem. B* **2005**, *109*, 21015. (b) Mu, Z. C.; Shu, L. J.; Fuchs, H.; Mayor, M.; Chi, L. F. *J. Am. Chem. Soc.* **2008**, *130*, 10840. (c) Kampschulte, L.; Lackinger, M.; Maier, A. K.; Kishore, R. S. K.; Griessl, S.; Schmittel,

M.; Heckl, W. M. *J. Phys. Chem. B* **2006**, *110*, 10829. (d) Kampschulte, L.; Werblowsky, T. L.; Kishore, R. S. K.; Schmittel, M.; Heckl, W. M.; Lackinger, M. *J. Am. Chem. Soc.* **2008**, *130*, 8502.
(17) (a) Kampschulte, L.; Griessl, S.; Heckl, W. M.; Lackinger, M. *J. Phys. Chem. B* **2005**, *109*, 14074. (b) Ziener, U.; Lehn, J.-M.; Mourran, A.; Möller, M. *Chem.—Eur. J.* **2002**, *8*, 951. (c) Zhang, J.; Li, B.; Cui, X. F.; Wang, B.; Yang, J. L.; Hou, J. G. *J. Am. Chem. Soc.* **2009**, *131*, 5885.
(18) Dunitz, J. D.; Gavezzotti, A. *Angew. Chem., Int. Ed.* **2005**, *44*, 1766.
(19) Palma, C.-A.; Cecchini, M.; Samorì, P. *Chem. Soc. Rev.* **2012**, *41*, 3713.
(20) (a) Palma, C. A.; Samorì, P.; Cecchini, M. *J. Am. Chem. Soc.* **2010**, *132*, 17880. (b) Linares, M.; Minoia, A.; Brocorens, P.; Beljonne, D.; Lazzaroni, R. *Chem. Soc. Rev.* **2009**, *38*, 806.
(21) (a) Lin, N.; Stepanow, S.; Ruben, M.; Barth, J. V. *Top. Curr. Chem.* **2009**, *287*, 1. (b) Ma, X.-J.; Yang, Y.-L.; Deng, K.; Zeng, Q.-D.; Wang, C.; Zhao, K.-Q.; Hu, P.; Wang, B.-Q. *ChemPhysChem* **2007**, *8*, 2615. (c) Ciesielski, A.; Stefankiewicz, A. R.; Hanke, F.; Persson, M.; Lehn, J.-M.; Samorì, P. *Small* **2011**, *7*, 342.
(22) (a) Szabelski, P.; De Feyter, S.; Drach, M.; Lei, S. B. *Langmuir* **2010**, *26*, 9506. (b) Tahara, K.; Ghijsens, E.; Matsushita, M.; Szabelski, P.; De Feyter, S.; Tobe, Y. *Chem. Commun.* **2011**, *47*, 11459. (c) Szabelski, P.; De Feyter, S. *CrystEngComm* **2011**, *13*, 5542. (d) Lei, S. B.; Tahara, K.; Müllen, K.; Szabelski, P.; Tobe, Y.; De Feyter, S. *ACS Nano* **2011**, *5*, 4145. (e) Adisoejoso, J.; Tahara, K.; Lei, S. B.; Szabelski, P.; Rżysko, W.; Inukai, K.; Blunt, M. O.; Tobe, Y.; De Feyter, S. *ACS Nano* **2012**, *6*, 897.
(23) (a) Lei, S. B.; Tahara, K.; De Schryver, F. C.; Van der Auweraer, M.; Tobe, Y.; De Feyter, S. *Angew. Chem., Int. Ed.* **2008**, *47*, 2964. (b) Mali, K. S.; Adisoejoso, J.; Ghijsens, E.; De Cat, I.; De Feyter, S. *Acc. Chem. Res.* **2012**, *45*, 1309.
(24) Chakrabarty, R.; Mukherjee, P. S.; Stang, P. J. *Chem. Rev.* **2011**, *111*, 6810.
(25) Ecija, D.; Vijayaraghavan, S.; Auwärter, W.; Joshi, S.; Seufert, K.; Aurisicchio, C.; Bonifazi, D.; Barth, J. V. *ACS Nano* **2012**, *6*, 4258.
(26) (a) Lee, S. J.; Mulfort, K. L.; O'Donnell, J. L.; Zuo, X. B.; Goshe, A. J.; Wesson, P. J.; Nguyen, S. T.; Hupp, J. T.; Tiede, D. M. *Chem. Commun.* **2006**, 4581. (b) Mongin, O.; Papamicaël, C.; Hoyler, N.; Gossauer, A. *J. Org. Chem.* **1998**, *63*, 5568.
(27) (a) Becke, A. D. *J. Chem. Phys.* **1993**, *98*, 5648. (b) Lee, C. T.; Yang, W. T.; Parr, R. G. *Phys. Rev. B* **1988**, *37*, 785.
(28) Lukin, O.; Leszczynski, J. *J. Phys. Chem. A* **2002**, *106*, 6775.
(29) Frenkel, D.; Smit, B. *Understanding Molecular Simulation*; Academic Press: London, 2002.
(30) Tarini, M.; Cignoni, P.; Montani, C. *IEEE Trans. Visualization Comput. Graphics* **2006**, *12*, 1237.
(31) Mu, Z. C.; Shu, L. J.; Fuchs, H.; Mayor, M.; Chi, L. F. *J. Am. Chem. Soc.* **2008**, *130*, 10840.